FRONT SURFACE PASSIVATION OF N-TYPE HIGH-EFFICIENCY BACK-JUNCTION SILICON SOLAR CELLS USING FRONT SURFACE FIELD

F. Granek[1], C. Reichel[1], M. Hermle[1], D. M. Huljić[2], O. Schultz[1], S.W. Glunz[1]
[1]Fraunhofer Institute for Solar Energy Systems, Heidenhofstr. 2, D-79110 Freiburg, Germany
Phone: +49-761-4588-5287; Fax: +49-761-4588-9250; email: filip.granek@ise.fraunhofer.de
[2]Q-Cells AG, Guardianstr. 16, 06766 Bitterfeld-Wolfen (OT Thalheim), Germany

ABSTRACT: Front surface passivation of back-junction back-contact *n-type* Si solar cell structure was analysed. Passivation quality of the phosphorus diffused front surface field, thin thermal oxide and antireflection silicon nitride was investigated. Surface saturation current densities (J_{0s}) of textured and untextured n^+nn^+ test samples with different n^+ phosphorus diffusion profiles were measured under high and low injection for two sample base resistivities. Surface saturation current densities determined under high and low injection are in a very good agreement. For the untextured surfaces the best J_{0s} of 6 fA/cm^2 without the front surface field diffusion and 20 fA/cm^2 with shallow lowly doped front surface field were measured. J_{0s} of 31 fA/cm^2 and 27 fA/cm^2 for textured samples with and without the front surface field respectively were measured. These low surface saturation current densities of textured samples results in V_{OC} limits higher than 705 mV.
Keywords: c-Si, Back-Contact, High-Efficiency, n-type

1 INTRODUCTION

The back-contact and back side collecting silicon solar cell design represents a very attractive cell structure, which already demonstrated efficiency better than 21% in production lines [1] (for comparison the today standard solar cells have the efficiency of 16-18%). At Fraunhofer ISE in a cooperation with Q-Cells AG and ISFH we are developing a back-contact back-junction solar cell structure. Efficiencies up to 21% [2] with *n-type* CZ-Si on small cell areas were already achieved and up-scaling to large cell areas is in progress.

The focus of this paper is the front side passivation of the solar cell structure that we presently develop. We analysed the influence of the different front surface field (FSF) phosphorus dopant profiles on the surface saturation current for the textured and untextured surfaces passivated with thin thermal oxide and antireflection PECVD silicon nitride coating. We investigated the front surface passivation using thin thermal oxide and antireflection silicon nitride as this technology is industrially relevant and will allow for good cell performance after module assembly, in contrast to a thick 105 nm antireflection oxide passivation.

2 FRONT SIDE PASSIVATION OF THE BACK-JUNCTION BACK-CONTACT CELLS

In the solar cell most of the photogeneration occurs at the front cell side, where the light-generated carriers can easily be lost by recombining at a poorly passivated surface instead of reaching the *p-n* junction, which in case of the back-juntion cell structure is located on the back cell side. That is why excellent front surface passivation is one of the most important requirements of the back-junction cell type.

In Fig. 1 the influence of the front surface recombination velocity ($S_{0,front}$) on the back-junction back-contact cell performance is shown. PC1D [3] simulations show the importance of excellent front surface passivation for a back-junction cell. With increasing $S_{0,front}$ the efficiency of the cells without FSF decreases rapidly. Cells with FSF profit from the reduction of the effective recombination velocity in broader $S_{0,front}$ range.

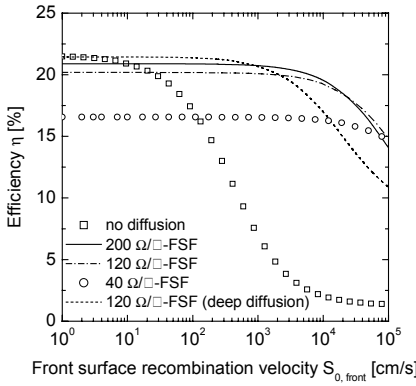

Figure 1: Influence of the front surface recombination velocity ($S_{0,front}$) on the efficiency of the back-junction *n-type* Si solar cells with different FSF diffusion profiles (one-dimensional PC1D simulations).

The influence of the front side recombination velocity is visible in the whole wavelength range of the internal quantum efficiency of the back-junction cells (figure 2). That is why the reduction of the front surface recombination is of high importance for the discussed cell type.

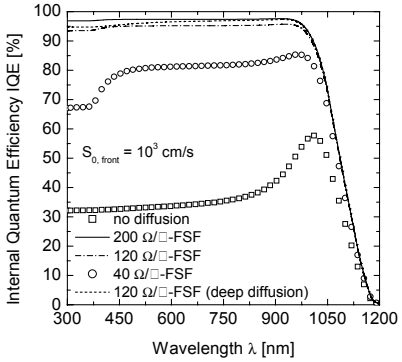

Figure 2: Internal quantum efficiency of a *n-type* back-junction solar cells for different front surface field diffusion profiles. $S_{0,\ front}$ of 1000 cm/s was assumed for this PC1D simulations.

Maxeon EX2015
CSI v. Maxeon
IPR2024-01194

Some other advantages of using a front surface field are: (a) the reduction of the series resistance for the majority carriers which need to travel long distances laterally in order to reach base contact [4], (b) increased long term UV-stability of the passivation in contrast to surfaces passivated with oxide and without the FSF [5].

King [6] and Cuevas [7] have studied the saturation current densities of the phosphorus doped emitters. In their work the Gaussian phosphorus profiles were analysed. In our work the focus is to analyse the error-function n^+ profiles, which are relevant to the cell structure with very thin thermal oxide passivation. In contrast to both authors we studied the n^+nn^+ samples with front surface field, without the *p-n* junction.

3 SAMPLE PREPARATION

n^+nn^+ symmetrical test sturctures for the lifetime measurements (see figure 3) were processed on 250 µm thick *n-type* FZ-Si wafers. Base resistivity of 1 and 10 Ω cm was selected for this study. This base resistivity range is interesting for the manufacturing of the high-efficiency back-junction back-contact solar cells. The advantage of using high quality *n-type* FZ-Si is the very high bulk lifetime. In our previous study we measured carrier lifetimes for this material of 1.2 ms for 1 Ω cm and 10.1 ms for 10 Ω cm base resistivity [8]. Due to these high carrier lifetimes, the recombination in bulk material is only minimal, and the carrier lifetime is limited only by the surface recombination. This way a good determination of the surface recombination effects is possible.

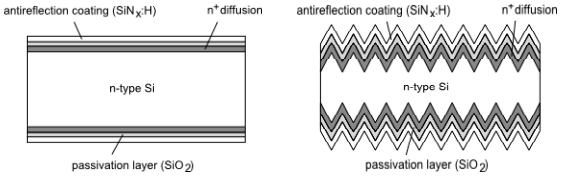

Figure 3: n^+nn^+ symmetrical test structures for the lifetime measurements and the dermination of the surface recombination current density. The test structures with textured and untextured surfaces were processed.

Test samples with untextured and textured surfaces (random pyramids) were processed. The front surface field (FSF) was created on both sample sides by a tube furnace phosphorus diffusion form liquid $POCl_3$ source. Phosphorus diffusion temperature was varied in the range of 780-840°C. It resulted in different n^+ error-function dopant profiles (see figure 4). Phosphorus glass was etched back in HF solution. For selected samples a deep Gaussian phosphorus profile (called 'deep diffusion') was created by a dry thermal oxidation at 1050°C to form a 105 nm thick antireflection SiO_2 layer. The high oxidation temperature caused redistribution of the phosphorus atoms and transition from the error-function dopant profile to Gaussian profile. The thick oxide was then etched-back in HF solution. Next, the thermal oxide of the goal thickness of about 10 nm for the passivation of the silicon surface was grown during a short dry oxidation at 850°C. Due to the short oxidation time and its low temperature, the doping profiles were not changed significantly. All wafers were processed in one oxidation step, and the oxide growth rate is different on differently doped surfaces. This resulted in the oxide thickness variation of all samples in the range of 10-40 nm. Next, the antireflection 70 nm thick PECVD silicon nitride coating was deposited. Finally all samples were annealed at forming gas atmosphere (FGA) at 425°C (15 min.).

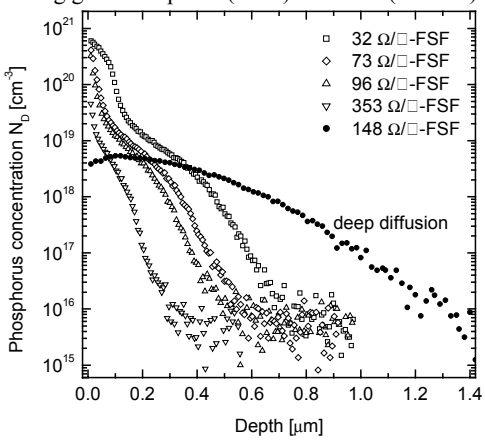

Figure 4: Secondary ion mass spectometry (SIMS) profiles of the studied phosphorus dopant profiles measured for untextured samples after all high temperature processing steps. Sheet resistance FSF was calculated by integrating the dopant profiles using the mobility model from Masetti [9].

4 DETERMINATION OF THE SURFACE SATURATION CURRENT

4.1 Injection dependent lifetime measurements

We measured the lifetime of all samples in a wide injection density range with the quasi-steady–state photo-conductance (QSSPC) method [10]. Measurements were done using WTC-120 lifetime tester from Sinton Consulting. The sample temperature during the measurements was set to 30°C (303 K). For the calculation of recombination parameters we used the intrinsic carrier concentration value $n_i = 1.3 \times 10^{10}$ cm^{-3} (303 K) calculated as in [11]. The same n_i value was used for both base resistivities. Because of the different SiO_2 thicknesses of samples with different n^+ dopant profile, the optical factor required for QSSPC measurements had to be calculated for all samples. After measuring the oxide thickness, the optical factor was calculated using the *SUNRAYS* software [12].

In order to determine the surface saturation current density (J_{0s}) two methods were applied. We determined J_{0s} under low level injection for 1 Ω cm samples (section 4.2) and under high level injection for 10 Ω cm samples (section 4.3). This way a direct comparison of J_{0s} values determined by both methods was possible.

Next to J_{0s}, the V_{OC} limit (equation 1) imposed by $J_0 = 2 \times J_{0s}$ was calculated for all determined J_{0s} ($J_{SC} = 40$ mA/cm^2 was assumed). For calculation of $V_{OC,\,Limit}$ the same temperature (303K) as for measurements of the J_{0s} was taken. The $V_{OC,\,Limit}$ is the maximal V_{OC} that can be achieved with the used passivation of both surfaces (influence of the bulk recombination was neglected in calculation of $V_{OC,\,Limit}$).

$$V_{OC,\,Limit} = \frac{kT}{q}\ln\left(\frac{J_{SC}}{J_0}+1\right) \qquad (1)$$

4.2 Determination of J_{0s} under low injection

The effective lifetime τ_{eff} measured under low level

injection at $\Delta n = 1 \times 10^{14}$ cm^{-3} was taken for the calculations. For 1 Ω cm samples $N_D = 5 \times 10^{15}$ cm^{-3} satisfies the low level injection condition ($\Delta n << N_D$). Surface lifetime τ_s was calculated using the equation (2). For the bulk lifetime τ_b the intrinsic Auger and radiative recombination was used. For the calculation of the Auger lifetime the model of Kerr [13] was used. Neglecting the Shockley-Read-Hall bulk recombination resulted in the determination of the upper limit for J_{0s} value:

$$\frac{1}{\tau_{eff}} = \frac{1}{\tau_b} + \frac{1}{\tau_s} \qquad (2)$$

For our symetrical lifetime samples, S_{eff} can now be calculated using a very good approximation from Sproul [14]:

$$\tau_s = \frac{W}{2S_{eff}} + \frac{1}{D}\left(\frac{W}{\pi}\right)^2 \qquad (3)$$

With the known S_{eff} value the J_{0s} can then be calculated using equation 4:

$$S_{eff} = \frac{J_{0s}\left(N_D + \Delta n\right)}{qn_i^{\,2}} \qquad (4)$$

In figure 5 examples of the measured lifetime curves over a broad injection level are shown.

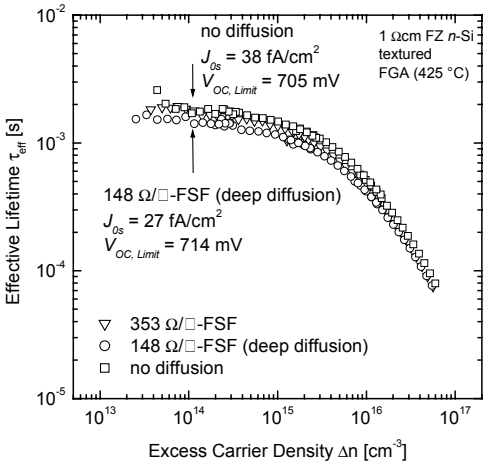

Figure 5: Example of QSSPC lifetime measurements of the textured 1 Ω cm test samples. J_{0s} and $V_{OC, Limit}$ determined at $\Delta n = 1 \times 10^{14}$ cm^{-3} are shown for sample without the FSF diffusion and for sample with 148 Ω/sq. deep Gaussian diffusion profile.

4.3 Determination of J_{0s} under high injection

Under high injection ($\Delta n >> N_D$) the recombination of the diffused surfaces together with Auger recombination limits the effective lifetime. One can analyse the inverse effective lifetime corrected for the Auger recombination limit under high injection with the so called *'slope method'* proposed by Kane [15]. The slope of the inverse lifetime is then proportional to $2 \times J_{0s}$ according to equation:

$$\frac{1}{\tau_{eff}} - \frac{1}{\tau_A} = \frac{1}{\tau_{SRH}} + \frac{2J_{0s}}{qn_i^{\,2}W}\Delta n \qquad (5)$$

The 10 Ω cm samples ($N_D = 4.5 \times 10^{14}$ cm^{-3}) could be easily measured in high injection. We calculated the slope of the inverse lifetime curve at $\Delta n_{hli} = 10 \times N_D$. Auger coefficient $C_A = 1.66 \times 10^{-30}$ cm^{-3}s^{-1} [16] was used for the calculation of the Auger lifetime term ($\tau_A^{-1} = C_A \Delta n^2$). For the determination of the slope of the inverse lifetime curve, we performed the linear fit with measured data points form the range of $\Delta n_{hli} \pm 0.8 \times \Delta n_{hli}$. Examples of the determination of J_{0s} for the textured 10 Ω cm test samples under high injection are shown in figure 6.

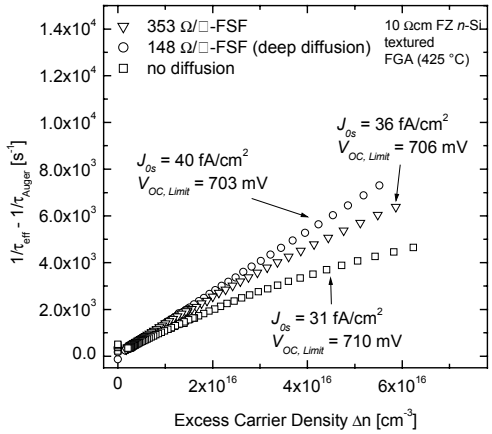

Figure 6: Determination of J_{0s} in high injection using the 'slope method'. Examples of the determined J_{0s} and $V_{OC, Limit}$ for the textured 10 Ω cm samples are shown.

5 SURFACE SATURATION CURRENT DENSITY FOR SAMPLES WITH DIFFERENT n^+ DOPING

5.1 J_{0s} for different phosphorus diffusion profiles

Determined J_{0s} values together with $V_{OC, Limit}$ are summarized in Table I (untextured samples) and Table II (textured samples). We observed a very good agreement between J_{0s} as determined under high injection using the slope method for the 10 Ω cm samples and in low injection for the 1 Ω cm samples. This shows that both methods enable very good determination of J_{0s} of the samples with front surface field. The presence of *p-n* junction is not required to determine the recombination currents of the n^+ diffused regions [7]. Both methods of determination of J_{0s} proved also to be independent of the base doping.

Table I. Summary of the results for the untextured samples with different front surface field diffusions.

	ρ_{base} = 1 Ω cm low-level-injection		ρ_{base} = 10 Ω cm high-level-injection	
n^+ diffusion [Ω/sq.]	J_{0s} [fA/cm^2]	$V_{OC, Limit}$ [mV]	J_{0s} [fA/cm^2]	$V_{OC, Limit}$ [mV]
32	721	628	740	627
73	210	660	229	658
96	109	677	124	674
353	20	722	22	719
148 (deep)	22	719	26	714
no diffusion	6	753	6	753

Extremly low J_{0s} = 6 fA/cm^2 for the non-diffused surface were measured. This proves that the thin (10 nm) thermal oxide and PECVD SiN_X (70 nm) passiavtion is very effective. Phosphorus diffusion introduces Auger recombination and recombination due to crystal defects. That is why J_{0s} of samples with FSF are higher than for

samples without FSF for the untextured surfaces. Of the investigated diffusions deep Gaussian diffusion (148 Ω/sq.) and shallow error-function (353 Ω/sq.) diffusion result as expected in the lowest J_{0s} values. These are the two dopant profiles with the lowest surface phosphorus concentration.

Strong J_{0s} dependence of the sheet resistance is shown in figure 7. J_{0s} of the error-function diffusions could be very well fitted with linear fit in the broad sheet resistance range. Deep Gaussian diffusion seems to have a different dependence of the ρ_{sheet}. This may be due to differences in surface phosphorus concentration.

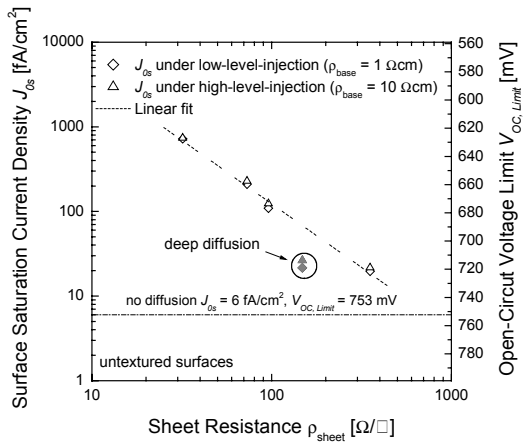

Figure 7: J_{0s} and $V_{OC, Limit}$ as a function of sheet resistance of the n^+ diffusion for the untextured samples. J_{0s} of the sample without FSF is shown for comparison.

For textured surfaces (Table II) J_{0s} is as expected higher than for the untextured samples. This is due to larger surface area of the textured samples and could also be caused by a different phosphorus concentration at the tops and bottoms of the pyramids. For the textured samples with FSF the V_{OC} higher than 705 mV are possible. Such a good surface passivation with thin SiO_2 and antireflection SiN_X layers should enable processing of high-efficiency back-junction back-contact solar cells.

Table II. Summary of the results for the textured samples with different front surface field diffusions.

	ρ_{base} = 1 Ω cm low-level-injection		ρ_{base} = 10 Ω cm high-level-injection	
n^+ diffusion [Ω/sq.]	J_{0s} [fA/cm²]	$V_{OC, Limit}$ [mV]	J_{0s} [fA/cm²]	$V_{OC, Limit}$ [mV]
32	1170	615	1180	615
73	290	651	296	651
96	138	671	161	667
353	31	710	36	706
148 (deep)	38	705	40	703
no diffusion	27	714	31	710

6 CONCLUSIONS

A high quality of the front surface passivation is very important for the back-junction back-contact solar cell type. Our PC1D simulations show that without the appropriate front surface passivation, efficiencies above 20% can not be reached. Application of phosphorus diffused front surface field enables high efficiencies even at not perfectly passivated silicon front surfaces. This is not possible without the front surface field.

Surface saturation current densities of the textured and untextured *n-type* test samples with different n^+ diffusion profiles were measured under high and low injection for 1 and 10 Ω cm base resistivity. Both methods enabled determination J_{0s} of the n^+nn^+ test samples. J_{0s} determined under high and low injection are in a very good agreement.

Very low J_{0s} of the samples passivated with thin thermal oxide and antireflection SiN_X were measured. For the untextured surfaces the best J_{0s} of 6 fA/cm² without the FSF diffusion and 20 fA/cm² with shallow lowly doped front surface field were measured. For the textured samples J_{0s} of 27 and 31 fA/cm² for samples without and with front surface field, respectively, were measured. Such a low surface saturation current of the textured surfaces results in V_{OC} limit higher than 705 mV. This high quality of the front surface passivation with front surface field should enable processing of the high-efficiency *n-type* back-junction back-contact silicon solar cells.

ACKNOWLEDGEMENTS

This work is supported by the German Federal Ministry for the Environment, Nature Conservation and Nuclear Safety in the frame of the QUEBEC project (FKZ 0329988). The authors thank T. Leimenstoll and S. Seitz for sample processing and J. Benick for valuable discussions.

REFERENCES

[1] W. P. Mulligan *et al.*, Proc. 19th EU-PVSEC, Paris, France (2004) .
[2] D. M. Huljic *et al.,* Proc. 21st EU-PVSEC, Dresden, Germany (2006) .
[3] D. A. Clugston and P. A. Basore, Proc. 26th IEEE PVSC, Anaheim, USA (1997) 207-210.
[4] J. Dicker *et al.,* Proc. 28th IEEE PVSC, Anchorage (2000).
[5] P. E. Gruenbaum, R. A. Sinton, R. M. Swanson, Proc. 20th IEEE PVSC, Las Vegas, USA (1988) 323-428.
[6] R. R. King, R. A. Sinton and R. M. Swanson, IEEE Trans. Electron Devices, 37, (1990), 365-371.
[7] A. Cuevas, P. A. Basore, G. Giroult-Malakowski, C. Dubois, J. Appl. Phys., 80, (1996), 3370-3375.
[8] F. Granek, M. Hermle, B. Fleischhauer, A. Grohe, O. Schultz, S. W. Glunz, G. Willeke, Proc. 21th EU-PVSEC, Dresden, Germany (2006) 777-780.
[9] G. Masetti, M. Severi, S. Solmi, IEEE Trans. Electron Devices, 30, (1983), 764.
[10] R. A. Sinton, A. Cuevas and M. Stuckings, Proc. 25th IEEE PVSC, Washington DC, USA (1996) 457-460.
[11] M. A. Green, J. Appl. Phys., 67, (1990), 2944-2954.
[12] R. Brendel, Proc. 12th EU-PVSEC, Amsterdam, The Netherlands (1994), 1339.
[13] M. J. Kerr and A. Cuevas, J. Appl. Phys., 91, (2002), 2473.
[14] A. B. Sproul, J. Appl. Phys., 76, (1994), 2851-2854.
[15] D. E. Kane and S. M. Swanson, Proc. 18th IEEE PVSC, Las Vegas, USA (1985), 578-581.
[16] R. A. Sinton, R. M. Swanson, IEEE Trans. Electron Devices, 34, (1987), 1380-1389.

View publication stats